# Micelles from HOOC-PnBA-b-PAA-$C_{12}H_{15}$ diblock amphiphilic polyelectrolytes as protein nanocarriers

Aristeidis Papagiannopoulos[1,*], Anastasia Meristoudi[1], Stergios Pispas[1,*], Aurel Radulescu[2]

[1]Theoretical and Physical Chemistry Institute, National Hellenic Research Foundation, 48 Vassileos Constantinou Avenue, 11635 Athens, Greece.

[2]Jülich Centre for Neutron Science JCNS Forschungszentrum Jülich GmbH, Outstation at Heinz Maier-Leibnitz Zentrum (MLZ), 1 Lichtenbergstraße, 85747 Garching, Germany.

## ABSTRACT

We investigate the potential of self-assembled nanostructures of the PnBA-b-PAA amphiphilic diblock polyelectrolyte as candidates for drug delivery applications. Three PnBA-b-PAA copolymers with different molecular weights and PnBA/PAA weight ratios are tested. The system with the most well-defined core-shell micellar structure is chosen for complexation with lysozyme. Its solutions are found to contain well-defined core-shell micelles that are stable upon increase of solution salt content to physiological levels. Upon mixing with lysozyme we find that the protein globules accumulate preferably at the outer parts of the hydrated corona of the micelles. Increasing the protein concentration intermicellar aggregation is enhanced in a controllable way. At high salt content the number of proteins per micelle is lower compared to the low salt content, which points to an interaction of predominantly electrostatic nature. While light scattering is very sensitive to complexation, small angle neutron scattering is able to distinguish between the contributions from individual micelles and aggregates. This work

demonstrates the use of scattering techniques in order to characterize protein-polymer interactions in multiple hierarchical levels.

**KEYWORDS**

Amphiphilic polyelectrolytes, micelles, protein, small angle neutron scattering

## 1. INTRODUCTION

Block copolymer micelles are in the focus of intense research due to their potential for use in nano-scale encapsulation and drug delivery[1], bio-sensing and tissue engineering[2]. Their self-assembly and morphology have been extensively studied both experimentally and theoretically[3]. One class of self-assembled polymeric micelles are block polyelectrolyte micelles. They can be formed by diblock copolymers that contain one hydrophobic block and one polyelectrolyte block. In aqueous solutions the hydrophobic blocks of individual diblock chains form a core while the polyelectrolyte blocks extend towards the solution forming a hydrophilic charged corona[4]. Block polyelectrolyte micelles are responsive to salt content and pH when the polyelectrolyte contains weakly charged groups. Charged components like proteins bind to this kind of nanoparticles via electrostatic interactions[4], while hydrophobic drugs can be loaded into their core[5].

A variety of experimental techniques has been developed and upgraded in the last two decades for characterizing the loading and release on and from polyelectrolyte micelles in solution[6]. Small angle scattering techniques are non-invasive methods that are established for quantitative characterization of the morphology of nano-assemblies and their interactions with other components[7, 8]. The shape of micellar nanoparticles used for drug encapsulation and delivery may affect its loading and release properties[9, 10] and also its binding and internalization to cells[11].

Proteins contain “patches” of positive or negative charge and domains that may be hydrophilic or hydrophobic[6]. This way they interact with polyelectrolyte micelles via electrostatic and hydrophobic interactions. In amphiphilic block polyelectrolyte micelles the positioning of a loaded compound should be affected by the dominant interaction that causes the complexation i.e. a predominantly hydrophobic compound would be positioned on the core and a predominantly hydrophilic compound (e.g. charged) would stick on a polyelectrolyte chain of the corona[5].

In this work we use Small Angle Neutron Scattering (SANS)and Light Scattering (LS) to define the self-assembly of the diblock amphiphilic polyelectrolyte PnBA-b-PAA in three different molecular weights and block ratios, and their ability to form well-defined core-shell micelles in aqueous solutions. Furthermore, we use the optimal micellar architecture in order to make complexes with lysozyme. Our experiments allow us to define the core-shell structure of the micelles and their intemicellar aggregation state and the amount of complexed protein per micelle and its coarse-grain positioning on the core-shell structure. Electrophoretic Light Scattering (ELS) confirms the loading of the negatively charged PnBA-b-PAA micelles with the positively charged lysozyme globules. Static and Dynamic Light Scattering (SLS/DLS) support our small angle scattering findings and extend the investigation to lower concentrations. This study expands the detailed investigations of proteins in spherical polyelectrolyte brushes[12] (linear polyelectrolytes grafted on polystyrene nanoparticles) to proteins in self-assembled polyelectrolyte micelles.

## 2. EXPERIMENTAL

### 2.1 Materials

The diblock copolymers PnBA-b-PAA were synthesized by reversible addition fragmentation chain transfer radical polymerization technique (RAFT). Firstly, the PnBA homopolymer was synthesized in one step using 2-dodecylsulfanylthiocarbonylsulfanyl-2-methylpropionic acid as the CTA agent in the presence of AIBN as the polymerization initiator (moles CTA:AIBN = 5) at 65$^{o}$C over 15hrs in dioxane. The resulting homopolymer of the desired molecular weight was extracted by precipitation into excess solution of methanol/water (80%:20%) twice and dried in a vacuum oven. Then, the PnBA-b-PAA block copolymer was synthesized by using the PnBA block as the macroCTA agent and acrylic acid monomer. The synthesis occurred at 65$^{o}$C for 15hrs in the presence of AIBN (moles macroCTA:AIBN = 5) using dioxane as the solvent (scheme 1). The desired block copolymers were precipitated into hexane and were left to dry under vacuum prior to use. Overall yields for the diblocks were >90%. Their molecular characteristics are presented in Table 1, as derived by SEC and $^{1}$H-NMR (Supporting Information).

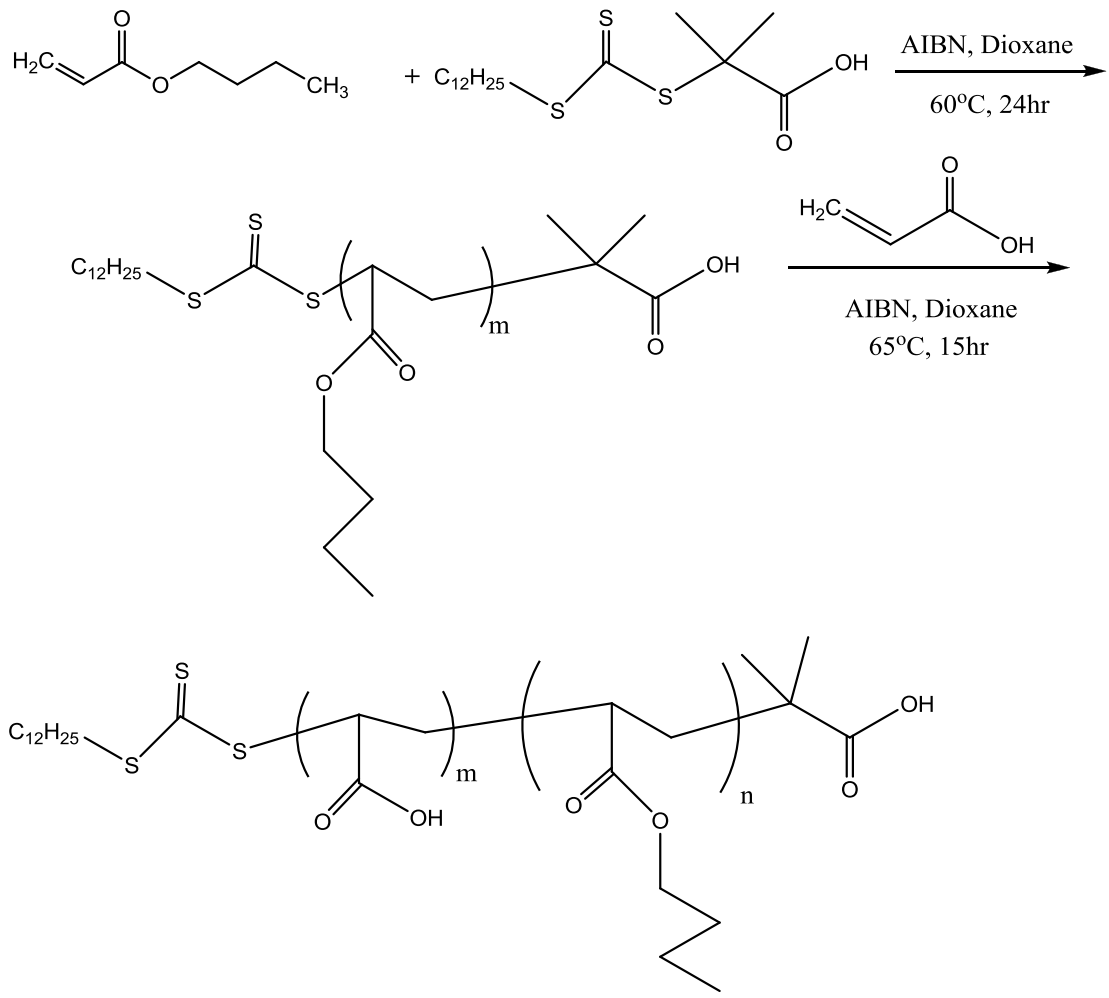


**Scheme 1**: Synthesis of PnBA-PAA block copolymer using RAFT methodology.

**Table 1.** Molecular characteristics of PnBA-b-PAA block copolymers utilized in this study

| Sample | $M_w$[a] x $10^{-4}$ (g $mol^{-1}$) | $M_w/M_n$[a] | %wt PnBA[b] | N $_{PnBA}$[c] | N $_{PAA}$[c] |
|---|---|---|---|---|---|
| PnBA-b-PAA-1 | 0.8 | 1.29 | 50 | 31 | 56 |
| PnBA-b-PAA-2 | 2.4 | 1.28 | 50 | 94 | 170 |
| PnBA-b-PAA-3 | 2.8 | 1.32 | 15 | 33 | 335 |

[a] by SEC in DMF

[b] by $^{1}$H-NMR in deuterated DMF

[c] degree of polymerization of each block

For small angle neutron scattering measurements aqueous solutions of mass concentration 3 mg/ml in aqueous solutions, were prepared by dissolving 30 mg of diblock copolymer in 3ml tetrahydrofuran (THF, from Fluka, UV spectroscopy grade) at 60°C for 5-6 hours. Subsequently, the THF solution was added rapidly to 10ml of $D_2O$ under vigorous stirring. THF was subsequently removed by evaporation at 65 ºC under stirring. This solution was used as a parent solution for the measurements. NaCl was used as a salt and NaOD or DCl for fixing the pH. The contribution of the added acid or base to the ionic strength was about $10^{-4}$ M hence it is negligible for our solutions were we use 0.01M and 0.15M NaCl for low and high (physiological) salt conditions. For light scattering the same preparation protocol was followed except from that the solvent was $H_2O$ and the pH-setting components were NaOH and HCl. Additionally, in order to avoid multiple scattering effects the target concentrations were low. Thus the parent solution was at a polymer content of 0.1mg/ml. For light scattering all sample solutions were filtered with 0.45μm PVDF membrane filters in order to remove any large aggregates or dust particles.

Hen egg white lysozyme (HEWL, $M_w$=14,700 g/mol) was purchased from Fluka and used without further purification. HEWL was dissolved at 0.3 mg/ml in $D_2O$ (pH7/0.01M) and 0.1mg/ml (pH7/0.01M salt) for SANS and LS respectively. The target concentrations were produced from the parent solutions by dilution in $D_2O$ or $H_2O$ (pH 7/0.01M salt). The lysozyme solutions were left overnight to equilibrate and for the isotopic exchange to take place in $D_2O$[13].

**2.2 Small Angle Neutron Scattering**

Small Angle Neutron Scattering (SANS) experiments were performed on the KWS-1 high resolution small angle neutron diffractometer, at the research reactor FRM II (Jülich Centre for Neutron Science). The nominal scattering vector ($q$) range is from 0.002 to 0.2 $Å^{-1}$(real space length scales ~1000 to 10 Å). This range was covered by three separate detection configurations (20, 8 and 2m sample-detector distance) at 4.7 Å wavelength. The SANS differential cross section is obtained by the scattered intensity $I(q)$ as a function of scattering wave-vector, $q = \frac{4\pi}{\lambda} sin\frac{\theta}{2}$, where $\lambda$ is the wavelength of the neutrons and $\theta$ is the scattering angle. The details on data collection, reduction and calibration and the convolution with the instrument's resolution function are described elsewhere[14, 15]. In the "Results and Discussion" section theoretically calculated scattered intensities are denoted in short as $I(q)$ although the convoluted scattered intensity is fitted to the experimental data. The temperature of the samples was set at 25 ºC by a Julabo thermostat with an accuracy of 0.01ºC.

**2.3 Static and Dynamic Light Scattering**

The experiments were performed on an ALV/CGS-3 compact goniometer system (ALVGmbH, Germany), equipped with a ALV-5000/EPP multi taudigital correlator and a He-Ne laser operating at the wavelength of 632.8 nm. In Static Light Scattering (SLS) the Rayleigh ratio $R(q)$was calculated with respect to a toluene standardat a series of angles in the range 30-120°. The scattering wave vector is given by $q = \frac{4\pi n_0}{\lambda} sin\frac{\theta}{2}$ where $n_0$ is the solvent's refractive index.

SLS data were treated[16] by the Zimm approximation:

$$\frac{Kc}{R(q,c)} = \frac{1}{M_w P(q)} \qquad (1)$$

where$q$ is the scattering wave vector, $M_w$ is the weight-averaged molar mass and $c$ is the particle concentration in solution. The single particle's form factor is given by $P(q) = e^{-\frac{1}{3}q^2 R_g^2}$(Guinier

approximation), where$R_g^2$ is the squared z-averaged radius of gyration. $K$ is the contrast factor for LS given by $K = \frac{4\pi^2 n_0^2}{N_A \lambda^4}(\partial n/\partial c)^2$, where $\partial n/\partial c$ is the refractive index increment of the scattering particles in the solvent.

In Dynamic Light Scattering (DLS) the intensity auto-correlation functions $g^{(2)}(t)$ are collected [17] at different scattering angles (30-120°) and can be analysed by the CONTIN algorithm. The characteristic relaxation rate $\Gamma(q)$ is taken from the position of the maximum ($\tau(q)$) of the distribution function of relaxation times ($\Gamma(q) = \frac{1}{\tau(q)}$). In the case of diffusive modes there is a linear relation between $\Gamma(q)$and $q^2$ i.e. $\Gamma(q) = D \cdot q^2$ and hence the diffusion coefficient $D$ is obtained. The hydrodynamic radius, $R_h$, is extracted from the Stokes-Einstein equation (equation 2).

$$R_h = \frac{k_B T}{6\pi\eta D} \qquad (2)$$

where $\eta$ is the viscosity of the solvent, $k_B$ is the Boltzmann constant and $T$ is the absolute temperature. All the LS experiments were performed at 25 ºC set by a PolyScience temperature controller.

### 2.4 Electrophoretic light scattering

Zeta potential measurements were performed on a Zetasizer Nano-ZS by Malvern Instruments Ltd.. The calculation was made by the Henry equation in the Smoluchowski approximation The $\zeta$ values reported are averages of 10-20 measurements taken at 173° angle. All the experiments were performed at room temperature.

## 3. RESULTS AND DISCUSSION

### 3.1 Self-assembly of PnBA-b-PAA in aqueous solutions

#### 3.1.1 Static and Dynamic Light Scattering

First we examined the aggregation behavior of the synthesized PnBA-b-PAA diblocks in aqueous media. It should be bared in mind that these copolymers carry hydrophobic $C_{12}$ groups at the free ends of the hydrophilic PAA blocks and single hydrophilic COOH groups at the free ends of the hydrophobic PnBA blocks. So their behavior in aqueous media is of interest since they resemble the case of ABCD quaterpolymers with very short end blocks of differing polarity relative to the corresponding large blocks to which they are attached. Typical SLS and DLS results from PnBA-b-PAA aqueous solutions are shown in figure 1. All the collected intensity autocorrelation functions were represented by a single mode in CONTIN analysis. The characteristic relaxation rate $\Gamma(q)$ (figure 1a) shows that PnBA-b-PAA-2 forms objects of low polydispersity in solution. In PnBA-b-PAA-1 there is evidence of polydisperse aggregates since $\Gamma$ vs $q^2$ plot presents an increasing slope i.e. at low $q$ large aggregates dominate the scattering while at high- $q$ small ones are the dominant species. PnBA-b-PAA-3 plot has a slope of about two times lower than the other two and additionally the three first data points present a very low slope. Possibly there are very large aggregates in coexistence with smaller ones (e.g. micelles) in solutions of PnBA-b-PAA-3.

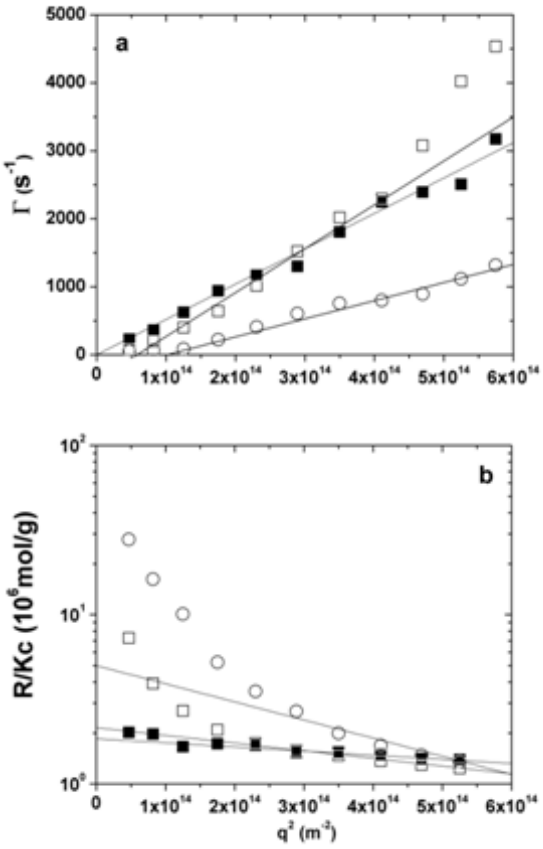


**Figure 1:** Light scattering data from 0.05mg/ml PnBA-b-PAA-1 (□), PnBA-bPAA-2 (■) and PnBA-b-PAA-3 (○) at pH7 and 0.15M NaCl. (a) Main relaxation rate as a function of $q^2$ (DLS). (b) Rayleigh ratio in Guinier plot (SLS). Straight lines are fits to the experimental data (at high q in the case of samples PnBA-b-PAA-1 and PnBA-b-PAA-3).

The Guinier plots (figure 1b) show high non-linearity for the case of PnBA-b-PAA-3. This is a sign of large aggregates (e.g. micellar aggregates) in solution in addition to any smaller ones(e.g. micelles). PnBA-b-PAA-1 solutions have a weaker low-q upturn which points to a less dominant presence of large aggregates. PnBA-b-PAA-2 has a linear Guinier plot. The $R_g$ and $Z_{agg}$ values in table 2 are obtained by the high- $q$ linear fit of the data (straight lines). The situation is similar for 0.01M NaCl (data not shown). The values of the radii obtained for PnBA-b-PAA-3 (table 2)

could be acceptable for micellar aggregates since the fully stretched size of its PAA chains[18] ($L = D_{PAA} \cdot 0.25nm \sim 80nm$) is not much smaller than $R_h$. But the strong evidence of large aggregates cannot be neglected and if the low-q region of the Guinier plot is used to estimate $R_g$ this will turn out much larger. In a similar manner the aggregation numbers ($Z_{agg}$) are strongly affected by the region that the linear fit is taken for PnBA-b-PAA-1 and PnBA-b-PAA-3. The LS results point out that PnBA-b-PAA-2 is possibly the system with the highest percentage of well-defined micelles so it is the best candidate between the three for protein loading. PnBA-b-PAA-1 apparently contains an increased amount of large aggregates whereas PnBA-b-PAA-3 is dominated by aggregates of various sizes. Larger multimicellar aggregates may be formed due to the presence of $C_{12}$ hydrophobic groups at the free ends of PAA blocks leading to intermicellar interaction between the micelles (scheme 1) and their effect is expected to be stronger in the case of sample PnBA-b-PAA-1 with the shorter PAA block[19]. Additionally the presence of a COOH group at the end of the PnBA block may induce some frustration to the core forming PnBA blocks since this group would like to be in contact with the aqueous phase and most probably would like to reside at the core-corona interface. This together with the low[20] $T_g$ (ca. -50 $^oC$) of the PnBA core forming blocks and their relative low hydrophobicity may alter the arrangement of the PnBA core blocks within the micelles in the copolymer systems under investigation, especially for samples PnBA-b-PAA-1 and PnBA-b-PAA-3 with the shorter PnBA block. Under the light of these observations PnBA-b-PAA-2 and PnBA-b-PAA-1 were tested with SANS for further determination of their structure in order to gain more information on the structure of the aggregates/micelles.

**Table 2:** SLS and DLS data from PnBA-b-PAA copolymers at 0.01 and 0.01M NaCl (pH 7).

| | 0.01 M | | | 0.15M | | |
|---|---|---|---|---|---|---|
| | PnBA-b-PAA-1 | PnBA-b-PAA-2 | PnBA-b-PAA-3 | PnBA-b-PAA-1 | PnBA-b-PAA-2 | PnBA-b-PAA-3 |
| $\boldsymbol{R_g\ (nm)}$ | 43±4 | 49±3 | 92±9 | 56±6 | 41±4 | 86±9 |
| $\boldsymbol{R_h(nm)}$ | 38±2 | 48±4 | 105±10 | 36±2 | 47±4 | 110±10 |
| $\boldsymbol{Z_{agg}}$ | 230±10 | 80±10 | 350±50 | 260±10 | 80±10 | 180±20 |

### 3.1.2 Small Angle Neutron Scattering from PnBA-b-PAA-2 and PnBA-b-PAA-1

The SANS data from PnBA-b-PAA-2 aqueous solutions (pH7, 0.01M and 0.15M NaCl) in several concentrations (figure 2) show a well-defined shoulder at $q = 0.04 - 0.05\text{Å}^{-1}$ which is characteristic sign of a form factor. At higher $q$ values a scaling law $I(q) \sim q^{-4}$ is the signature of scattering from objects with sharp boundaries. The scattering curves fall on top of each other with very good agreement when they are normalised by their corresponding concentration (data not shown) which reveals that the morphology observed is concentration-independent (in the concentration range under study with this technique).

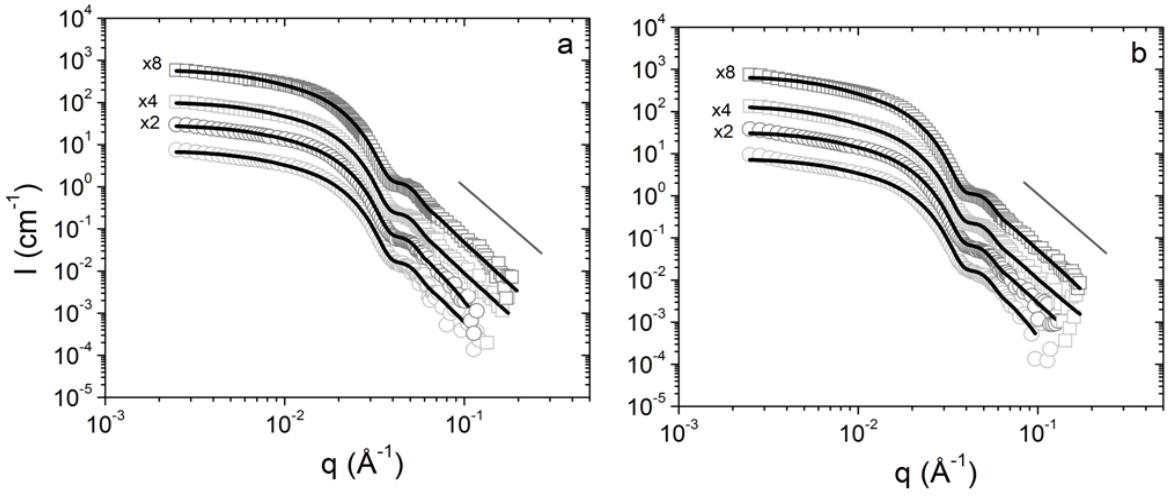

**Figure 2:** SANS profiles from PnBA-b-PAA-2 aqueous solutions 0.3mg/ml (○), 0.6mg/ml (○), 1mg/ml (□) and 3mg/ml (□) at pH7 with 0.01 (a) and 0.15 (b) M NaCl. Continuous lines are best fits with equation (3). The straight line indicates a power-law of $q^{-4}$. Data are multiplied by indicated factors for clarity.

The SANS data from PnBA-b-PAA-2 solutions were fitted by the core-shell micellar form factor[21, 22] as in equation 3. Polydispersity in core and micellar radius was introduced by a Gaussian distribution i.e. $I^{poly}(q;R) = \frac{\int_0^{+\infty} dR' \cdot exp\left(-\left(\frac{R'-R}{\sqrt{2}\Delta R}\right)^2\right) \cdot I(q;R')}{\int_0^{+\infty} dR' \cdot exp\left(-\left(\frac{R'-R}{\sqrt{2}\Delta R}\right)^2\right)}$ where $R$ is either the core or micellar radius. The optimized value of $\frac{\Delta R}{R}$ was at 17-18% for all our data.

$$I_{mic}(q) = N_{mic} \cdot \left\{4\pi \int_0^{\infty} \left(\rho(r) - \rho_{D_2O}\right) \cdot r^2 \frac{sin(qr)}{qr} \cdot dr\right\}^2 \qquad (3)$$

The neutron scattering length density profile $\rho(r)$ was modeled as the one of a uniform core of radius $R_c$ with the scattering length density of PnBA and a shell of radially varying volume fraction containing $D_2O$ and PAA of radius $R_m$ (equation 4). The neutron scattering length densities of the components were used as $\rho_{PnBA} = 0.65 \cdot 10^{-6}$Å$^{-2}$, $\rho_{PAA} = 2.70 \cdot 10^{-6}$Å$^{-2}$ and $\rho_{D_2O} = 6.40 \cdot 10^{-6}$Å$^{-2}$. The volume fraction profile is a power law i.e. $\varphi_{PAA}(r) = \varphi_0 \cdot \left(\frac{r}{R_c}\right)^{-a}$. From the fitted density profiles the number of PnBA blocks inside the core $Z_{mic}^{PnBA}$ and PAA blocks in the shell $Z_{mic}^{PAA}$ are calculated[14]. Combined with the number density of micelles $N_{mic}$ the mass concentration of micelles $c_{mic}$ is extracted.

$$\rho(r) = \begin{cases} \rho_{PnBA}\ for\ 0 \le r < R_c \\ \varphi_{PAA}(r) \cdot \rho_{PAA} - \left(1 - \varphi_{PAA}(r)\right) \cdot \rho_{D_2O}\ for\ R_c \le r < R_m \\ 0\ for\ R_m \le r < \infty \end{cases} \quad (4)$$

The number of blocks of PnBA and PAA in the core and in the shell (table 3) are in good agreement which means that the nanophase separation between hydrophobic and hydrophilic blocks is detected by SANS. In the case of 0.01M NaCl $Z_{mic}^{PAA}$ is lower than $Z_{mic}^{PnBA}$. This could be due to a mild collapse of PAA monomers on the hydrophobic core. A collapsed PAA layer has been assumed also in another work with diblock copolymers of the same chemical structure[18] but slightly different block lengths than ours. We have also supported the presence of such a collapsed layer made of a polyelectrolyte with hydrophobic backbone in contact with a hydrophobic core in a previous work[14]. At 0.15M the agreement is better possibly by the enhanced scattering at low q which is captured by the fits with an increase in the volume fraction in the shell. This may be caused by weak aggregation of micelles at higher salt concentration (weak upturn at the first 2-3 data points in figure 2b) due to screening effects. The aggregation numbers appear much higher than the ones in LS (about 80 for both 0.01M and 0.15M NaCl, table 2). The difference between the micellar aggregation numbers is possibly due to the differences in aggregation behavior in $H_2O$ and $D_2O$ and the concentration range that the micellization took place (stock solution concentrations: 0.1mg/ml in $H_2O$ and 3mg/ml in $D_2O$). Alternatively a possible loss of material during filtering (for SLS) could reduce the concentration of polymer in solution resulting to an apparently lower molecular weight.

$R_h$ values found for PnBA-b-PAA-2 (table 2) are lower compared to the $R_m$ values defined by SANS (tables 3). This is in accordance to the smaller micellar aggregation number $Z_{mic}$ found in SLS. The expected micellar radius is smaller in this case because of the reduced steric/electrostatic repulsion between PAA chains. The shell thickness $s = R_m - R_c$ is about $47nm$ for both salt contents. This length shows the extension of a PAA corona chain and compared to its contour length[18] which is $L = D_{PAA} \cdot 0.25nm$ we find that there are PAA chains in the corona that are fully stretched i.e. $\frac{s}{L} \approx 1$ .

The exponent $a \approx 3.2 - 3.3$ of the volume fraction profile is higher than the one expected from osmotic spherical polyelectrolyte brushes of strong ($a = 2$) or weak ($a = 8/3$) polyelectrolytes [23] [24]. This is a sign of PAA-PAA contacts that may be formed within the brush. The mass concentration of polymer is found near the nominal solution concentration (table 3) which confirms that most of the macromolecular chains in solution are incorporated into micelles. Overall the morphology of the PnBA-b-PAA-2 micelles appears very well-defined, independent of concentration and stable upon increase of salt content to physiological conditions. We have to keep in mind that PnBA forms a soft[18] core due to its low[20] glass transition temperature ($T_g^{PnBA} \approx -50$°C) but still it appears to form stable nanoparticles. The $R_g$ from SLS (table 2) is similar to $R_h$ (DLS). Normally one would expect the $R_g/R_h$ ratio to be significantly lower than unity (core-shell object) but it has been observed for core-shell micelles of a similar system[18] that the LS observed ratios can be near unity.

**Table 3:** Parameters obtained by SANS on the PnBA-b-PAA-2 solutions for several concentrations at pH 7.

| | **0.01M NaCl** | | | | **0.15M NaCl** | | | |
|---|---|---|---|---|---|---|---|---|
| **Parameter/ Concentration** | ***0.3mg/ml*** | ***0.6mg/ml*** | ***1mg/ml*** | ***3mg/ml*** | ***0.3mg/ml*** | ***0.6mg/ml*** | ***1mg/ml*** | ***3mg/ml*** |
| $\boldsymbol{R_c}$ $(\boldsymbol{nm})$ | 10.7±0.4 | 10.8±0.4 | 10.9±0.4 | 10.8±0.4 | 10.9±0.4 | 10.9±0.4 | 10.9±0.4 | 11.0±0.4 |
| $\boldsymbol{R_m}(\boldsymbol{nm})$ | 58±1 | 57±1 | 57±1 | 58±1 | 58±1 | 58±1 | 59±1 | 58±1 |
| $\boldsymbol{a}$ | 3.30±0.02 | 3.30±0.02 | 3.30±0.02 | 3.23±0.02 | 3.30±0.02 | 3.30±0.02 | 3.22±0.02 | 3.28±0.02 |
| $\boldsymbol{Z_{mic}^{PnBA}}$ | 260±6 | 268±6 | 272±6 | 271±6 | 272±6 | 273±6 | 272±7 | 272±6 |
| $\boldsymbol{Z_{mic}^{PAA}}$ | 226±6 | 212±6 | 214±6 | 236±6 | 221±8 | 253±8 | 263±8 | 282±8 |
| $\boldsymbol{c_{mic}}(\frac{\boldsymbol{mg}}{\boldsymbol{ml}})$ | 0.27±0.02 | 0.54±0.03 | 0.96±0.05 | 2.62±0.09 | 0.28±0.02 | 0.54±0.03 | 0.97±0.05 | 2.48±0.09 |

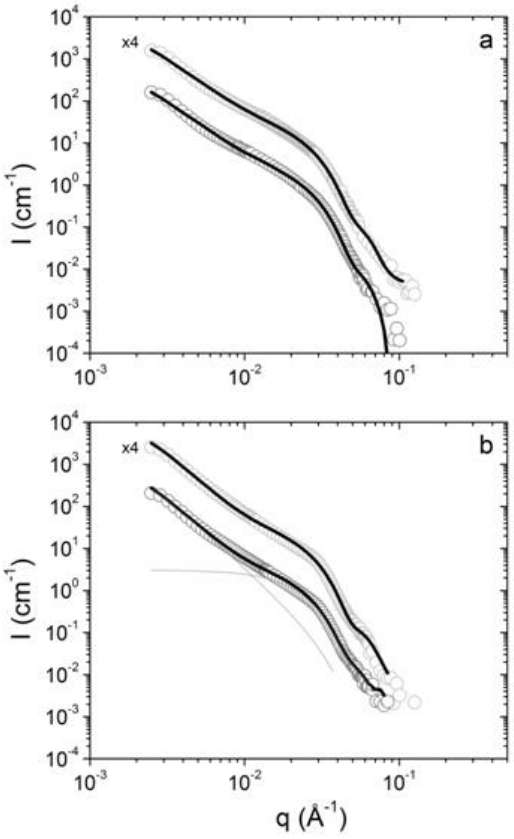


**Figure 3:** SANS profiles from PnBA-b-PAA-1 aqueous solutions 1 (○) and 3 (○) mg/ml at pH7, 0.01M NaCl (a) and 0.15M NaCl (b). Continuous lines are fits to the experimental data. The separate contributions of micelles and aggregates are shown in b.

The SANS data from PnBA-b-PAA-1 (figure 3) presented a power-law trend at $2x10^{-3}$-$2x10^{-2}$ Å$^{-1}$. This is a clear signature of micellar aggregation into larger clusters. Hence a superposition of $I_{mic}$ (equation 3) with a form factor of fractal aggregates $I_{agg}$ (equation 5) was used. Additionally a hydrated shell did not improve the fits and hence was removed. Due to strong aggregation the scattering at intermediate q is dominated by the aggregate form factor and the

contribution of the shell is unresolved. In any case PnBA-b-PAA-2 already appears as a less complex hierarchical system for detailed investigation of protein loading at this stage compared to PnBA-b-PAA-1.

$$I_{agg}(q) = G_{agg} \cdot exp\left(-\frac{q^2 R_g^2}{3}\right) + \frac{B_{agg}}{q^{d_{agg}}}\left[erf\left(\frac{qR_g}{\sqrt{6}}\right)\right]^{3d_{agg}} \qquad (5)$$

The prefactors[25] are related by $B_{agg} = \frac{G_{agg} \cdot d_{agg}}{R_g^{d_{agg}}} \cdot \left[\frac{6{d_{agg}}^2}{(2+d_{agg})(2+2d_{agg})}\right]^{d_{agg}/2} \Gamma\left(\frac{d_{agg}}{2}\right)$.

The contribution of aggregates is significant as the LS data have already shown. The radii $R_g$ and $R_h$ (table 2) are between 40 and 50 nm, while the expected micellar radius should be roughly three times lower than the one in PnBA-b-PAA-2. We have demonstrated the use of SANS to discriminate between well-defined micelles and fractal aggregates[21] in a recent publication and explained in detail the apparent radii obtained by LS. The concentration of micelles found by SANS (table 4) is in agreement with the polymer solution concentration, which means that the aggregates contain chains in micellar and not in another conformation. The micellar aggregation number is much higher compared to PnBA-b-PAA-2. Possibly the PnBA - PnBA hydrophobic interactions are more significant than the electrostatic attractions as the length of the blocks decreases. Fractal exponents are characteristic of mass fractal while at high salt content demonstrate denser aggregation (table 4).

Since PnBA-b-PAA-2 is the copolymer that provides solutions consisting of well-defined micelles with small number of coexisting aggregates, it was further tested for complexation with lysozyme.

**Table 4:** Parameters obtained by SANS on the PnBA-b-PAA-1 solutions for 1 and 3 mg/ml concentrations at 0.01 and 0.15M NaCl (pH 7).

| | ***0.01M*** | | ***0.15M*** | |
|---|---|---|---|---|
| | ***1mg/ml*** | ***3mg/ml*** | ***1mg/ml*** | ***3mg/ml*** |
| $\boldsymbol{R_c\ (nm)}$ | 8.7±0.3 | 8.7±0.3 | 8.2±0.3 | 8.6±0.3 |
| $\boldsymbol{Z_{mic}^{PnBA}}$ | 419±18 | 417±18 | 356±14 | 403±16 |
| $\boldsymbol{c_{mic}(\frac{mg}{ml})}$ | 1.16±0.05 | 3.31±0.09 | 1.21±0.05 | 3.23±0.09 |
| $\boldsymbol{d_{agg}}$ | 2.61±0.03 | 2.60±0.04 | 3.08±0.03 | 3.14±0.04 |

### 3.2 Complexation of PnBA-b-PAA-2 micelles with lysozyme

In figure 4 the SANS data from complexes of solutions of PnBA-b-PAA-2 mixed with lysozyme are shown. It is obvious that the scattering from aggregates (low-$q$ regime) is systematically enhanced by increasing the lysozyme content. At the intermediate-$q$ regime there is a less pronounced but yet clear systematic variation between the curves as a function of lysozyme content. This range corresponds to length scales in the outer layers of the micelles. At high $q$ the SANS form factor is unaltered by addition of lysozyme, showing that the concentrated interior (core) of the micelles is not affected and consequently the micelles do not lose their integrity upon complexation. The apparent drop of intensity at the characteristic oscillation for 0.15 M NaCl is rather caused by weak phase separation from solution of complexes at high salt content as will be discussed in the following. Indeed when a higher lysozyme/polymer mass ratio (10/10) was tested phase separation was visually evident and the scattered intensity vanished. Indeed the SANS-extracted micellar concentration $c_{mic}$ shows a weak drop as lysozyme is added for low salt content, whereas for the high salt case this drop is strong (tables 5 and 6).

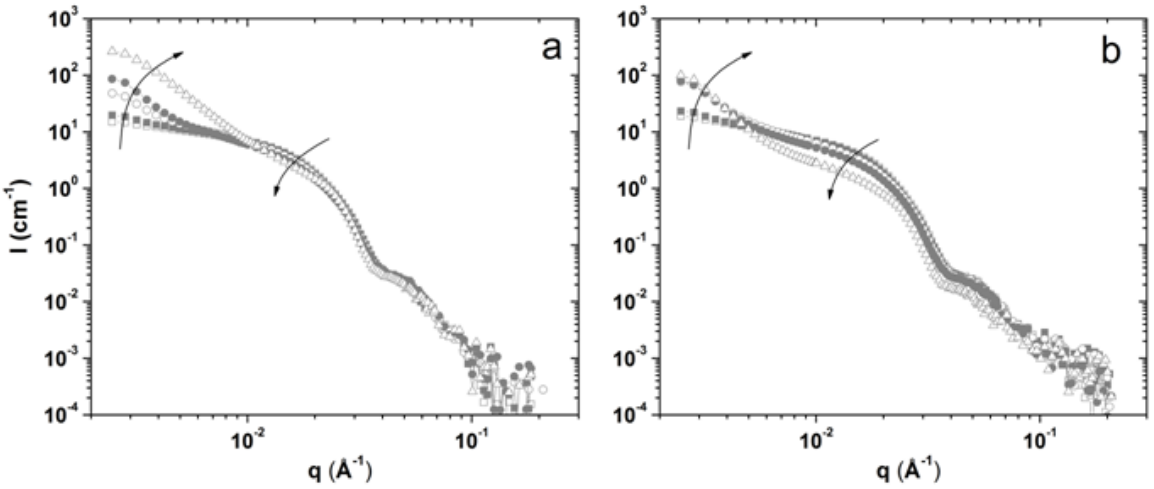


/

**Figure 4:** SANS profiles from lysozyme/PnBA-b-PAA-2 aqueous solutions 0.6 mg/ml at pH 7 0.01M (a) and 0.15M (b) NaCl with different mass ratios of lysozyme/polymer: 0/10 (□), 0.5/10 (■), 1/10 (○), 2/10 (●) and 4/10 (△).Curved arrows represent the direction of increasing lysozyme content.

The combined model of coexisting micelles and aggregates described by equations 3 and 5 was used to fit the SANS data from the PnBA-b-PAA/lysozyme complexes. Practically any other model for aggregate's scattering [26] or form factor [27] of well-defined objects (representing a separate species) would fit the data. The unified Guinier/power-law model appears to us as the most generic model for objects whose high-$q$ scattering cannot be resolved due to the domination of scattering from another species i.e. micelles in our case. Although our SANS data do not allow the detailed description of their form factor we cannot exclude that they may be another well self-organized species in coexistence with the core-shell micelles. Mixtures of spherical cylindrical micelles[28] and coexisting micelles with vesicles[29] have been found and analyzed in detail by SANS.

Representative fits for complexes at low and high salt content are shown in figure 5. Although the contribution from the aggregates is strong in comparison to the case of no added protein, the micellar form factor is still adequately separated from the aggregate form factor so that a detailed analysis of the core-micellar structure can be performed. The fitted parameters (tables 5 and 6) of the core and micelle radius remain the same (within experimental error) with the ones of the uncomplexed micelles (table 1) for both low and high salt content. This was expected by the fact (as mentioned above) that the shape of the SANS curves especially at high-$q$ was unaffected by the addition of lysozyme. Hence since the resulting $c_{mic}$ is consistent with the amount of polymer in solution the aggregates consist of micelles not significantly perturbed by clustering (loose aggregates). The systematic change in shape at intermediate length scales (micellar corona) is captured by a systematic drop of the density profile scaling exponent $a$. The effect of the reduced exponent is an apparent increase in the number of blocks within the corona. This is caused by attaching of lysozyme globules on PAA segments. Using the neutron scattering length density of lysozyme[30] in $D_2O$ $\rho_{lys} = 3.2 \cdot 10^{-6}\text{Å}^{-2}$ the excess apparent polymer mass is transformed to number of lysozyme globules per micelle $Z_{lys}$.

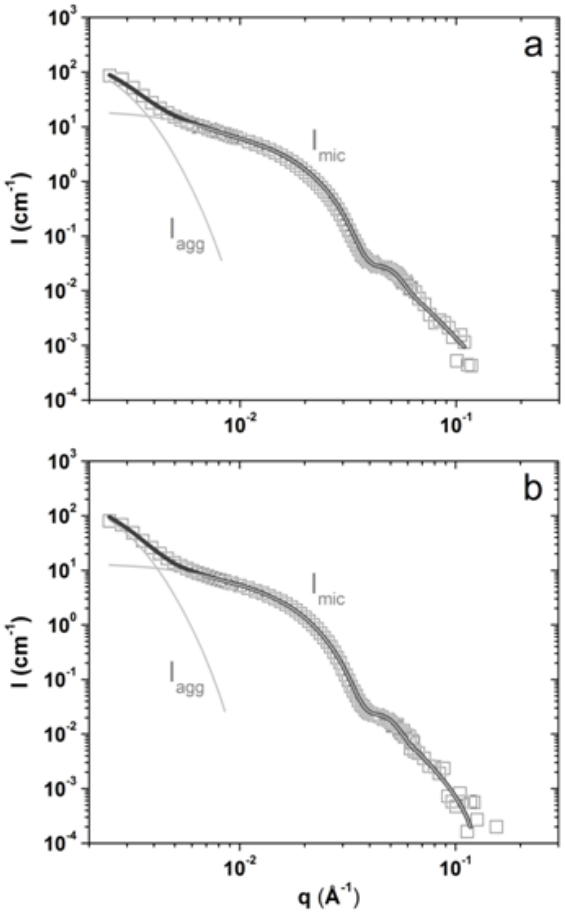


**Figure 5:** SANS profiles from PnBA-b-PAA-2 aqueous solutions 0.6 mg/ml at pH7 0.01M (a) and 0.15M (b) NaCl complexed with lysozyme at 2/10 lysozyme/polymer mass ratio. Continuous lines are fits to the experimental data. The separate contributions of micelles and aggregates are shown.

It would be possible for correlations between lysozyme globules attached on the micelles and correlations between these globules with the core and shell of the micelles to contribute to the scattering. In the case of the globule-globule correlations they should be found at length scales relevant to their hard-core diameter since no other form of ordering should exist within the micelles[12]. This corresponds to $q > 0.1\text{Å}^{-1}$ which is in the limits of our SANS window. The

globule-micelle correlations are determined by a factor $\frac{sin(qr)}{qr}$ averaged within the limits of the corresponding shell[12]. If the angular positioning of globules within the shells is random then in the ensemble of loaded micelles only the radial distribution of globules $p(r)\sim 4\pi r^2\varphi(r)$ contributes. The scattered intensity from our solutions of lysozyme in the absence of PnBA-b-PAA micelles at the lysozyme concentrations studied here is negligible in comparison to the scattering from micelles and complexes. Theoretically it is expected at $I_{lys} = N_{lys}V_{lys}^2\left(\rho_{lys} - \rho_{D_2O}\right)^2 \sim 0.01 cm^{-1}$, which is in the order of background scattering.

**Table 5:** Parameters obtained by SANS on the lysozyme/PnBA-b-PAA aqueous solutions 0.6 mg/ml at pH 7 and 0.01M NaCl with different mass ratios of lysozyme/polymer solutions.

| **Parameter/*** | **Lysozyme / Polymer mass ratio** | | | | |
|---|---|---|---|---|---|
| | ***0/10*** | ***0.5/10*** | ***1/10*** | ***2/10*** | ***4/10*** |
| $\boldsymbol{R_c\ (nm)}$ | 10.8±0.4 | 10.8±0.4 | 10.8±0.4 | 10.8±0.4 | 10.8±0.4 |
| $\boldsymbol{R_m(nm)}$ | 58±1 | 58±1 | 58±1 | 58±1 | 58±1 |
| $\boldsymbol{R_h(nm)*}$ | 49±3 | 43±3 | 35±3 | 37±3 | 36±3 |
| $\boldsymbol{R_g(nm)*}$ | 48±4 | 67±5 | 57±5 | 58±4 | 63±5 |
| $\boldsymbol{a}$ | 3.30±0.02 | 3.22±0.02 | 3.01±0.02 | 2.82±0.02 | 2.58±0.02 |
| $\boldsymbol{c_{mic}(\frac{mg}{ml})}$ | 0.54±0.03 | 0.52±0.03 | 0.49±0.03 | 0.49±0.03 | 0.45±0.03 |
| $\boldsymbol{Z_{lys}}$ | - | 19±2 | 59±5 | 117±13 | 185±14 |
| $\boldsymbol{Z_{lys}*}$ | - | 50±4 | 47±4 | 74±6 | 84±7 |
| $\boldsymbol{\zeta(mV)*}$ | -34±4 | -32±4 | -28±3 | -28±3 | -24±3 |

*parameters obtained from the LS experiments

**Table 6:** Parameters obtained by SANS on the lysozyme/PnBA-b-PAA aqueous solutions 0.6 mg/ml at pH7 and 0.15M NaCl with different mass ratios of lysozyme/polymersolutions.

| **Parameter/*** | **Lysozyme / Polymer mass ratio** | | | | |
|---|---|---|---|---|---|
| | ***0/10*** | ***0.5/10*** | ***1/10*** | ***2/10*** | ***4/10*** |
| $\boldsymbol{R_c\ (nm)}$ | 10.9±0.4 | 10.9±0.4 | 10.9±0.4 | 10.9±0.4 | 10.9±0.4 |
| $\boldsymbol{R_m(nm)}$ | 59±1 | 59±1 | 59±1 | 59±1 | 59±1 |
| $\boldsymbol{R_h(nm)*}$ | 47±4 | 34±3 | 31±3 | 31±3 | 34±3 |
| $\boldsymbol{R_g(nm)*}$ | 41±4 | 42±4 | 35±4 | 45±4 | 45±4 |
| $\boldsymbol{a}$ | 3.30±0.02 | 3.23±0.02 | 3.17±0.02 | 3.13±0.02 | 3.03±0.02 |
| $\boldsymbol{c_{mic}(\frac{mg}{ml})}$ | 0.54±0.03 | 0.53±0.03 | 0.48±0.03 | 0.39±0.03 | 0.23±0.03 |
| $\boldsymbol{Z_{lys}}$ | - | 22±1 | 47±4 | 52±4 | 58±4 |
| $\boldsymbol{Z_{lys}*}$ | - | 72±6 | 92±48 | 97±8 | 352±30 |
| $\boldsymbol{\zeta(mV)*}$ | -33±4 | -30±4 | -29±3 | -26±3 | -19±3 |

*parameters obtained from the LS experiments

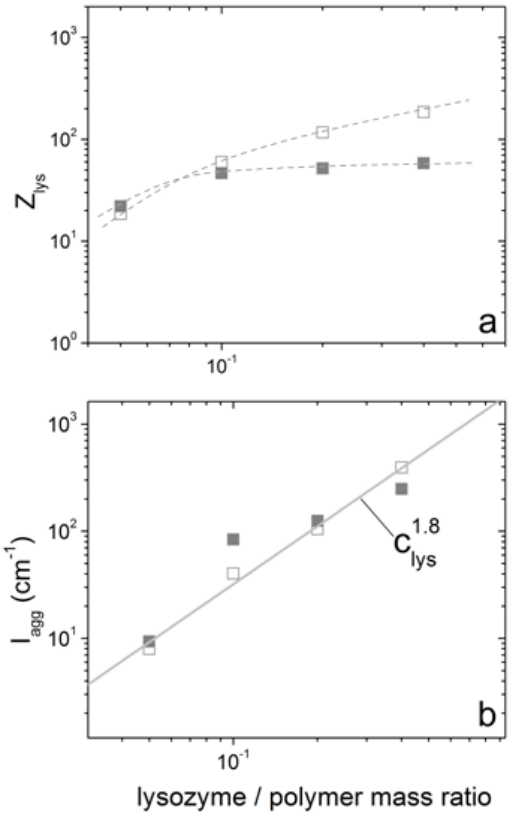


**Figure 6:** Number of lysozyme globules (a) and scattering intensity from aggregates (b) from PnBA-b-PAA-2 aqueous solutions 0.6 mg/ml complexed with lysozyme at pH7 0.01M (□) and 0.15M (■) NaCl. Dashed lines are guides to the eye. Straight line indicates the power law dependence.

A lysozyme globule has an ellispoid shape with a volume [31] that is less than 0.1% of the average shell volume of the PnBA-bPAA-2 micelles. Hence it can be thought of as a small particle entering a large polymeric structure. The number of lysozyme globules loaded per micelle obtained by SANS (figure 6a, tables 5 and 6) is an increasing function of protein concentration for low salt content, while in the case of high salt it apparently reaches a saturation value. This

shows that electrostatic interactions play a dominant role in the complexation between the two oppositely charged components[32]. In figure 6b the scattering contribution from aggregates at low q ($0.002\ \text{Å}^{-1}$) is presented. We have normalized this scattered intensity by the concentration of micelles obtained by SANS since its drop is most possibly caused by partial precipitation of complexes (tables 5 and 6). This effect is important at high salt content. The strong dependence on lysozyme concentration ($I_{agg} \sim c_{lys}^{1.8}$) highlights the sensitivity of the systems hiearchical organization. The protein globules may act as bridges between micelles. The decrease of the profile exponent $a$ upon complexation shows that protein globules adsorb preferentially on the micellar periphery. This way they are available to connect/complex with on the coronas of other micelles. The mass of lysozyme per micelle (data not shown) is comparable to this ratio in solution for low salt content which shows that micelles separate most of the protein from solution. We have observed the same effect in lysozyme interacting with poly(ethylene oxide)-block-poly(N-isopropylacrylamide)-block-poly(acrylic acid) (PEO-b-PNIPAM-b-PAA) thermoresponsive triblock copolymer aggregates at similar solution conditions. Following the kinetics of complexation secondary clustering of aggregates mediated by lysozyme was also observed[33]. At high salt free lysozyme globules remain in solution since complexation is weaker (figure 6a). One can conclude that keeping the protein solution content low provides a system with mostly loaded micelles and with weak presence of aggregates. Additionally the limits of strong aggregation and precipitation are explored by observing the morphology at higher protein contents.

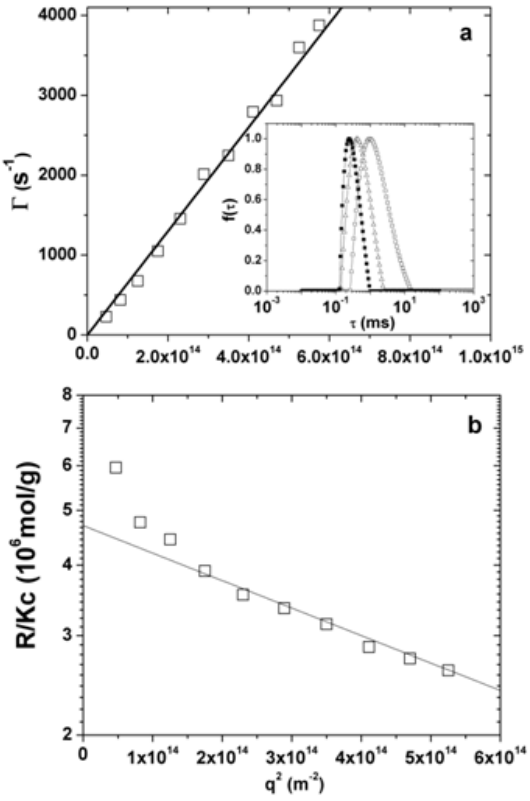


**Figure 7:** Light scattering from 0.05mg/ml PnBA-b-PAA-2 micelles at pH7 and 0.01M NaCl mixed with lysozyme at 2/10 lysozyme/polymer mass ratio. (a) Main relaxation rate as a function of $q^2$ (from DLS). Inset: relaxation time distributions obtained by CONTIN at 60° (○), 90° (△) and 120° (■). (b) Rayleigh ratio in Guinier plot (SLS). Straight lines are fits to the experimental data.

The light scattering results from PnBA-b-PAA-2 and their complexes are incorporated in tables 5 and 6. The hydrodynamic radii distributions extracted by CONTIN analysis contained in general one single diffusive mode and the relaxation rate $\Gamma(q)$ was found proportional to $q^2$ (figure 9a). The distributions of relaxation times are rather broad (figure 9a inset) and extend towards higher

relaxation times pointing to the presence of species of large hydrodynamic radius. This indicates intermicellar aggregation although less pronounced in very dilute solution. The static light scattering data (figure 9b) were analyzed with the Guinier approximation and contained non-linear behavior at low $q$ due to the presence of aggregates and hence the linear part of the plots was analyzed. Nevertheless a drop in $R_h$ is observed as protein content is increased (tables 5 and 6). In this case the number of PAA chains in the corona is small (~80) compared to the SANS experiments (~270). Hence incorporation of protein globules may induce folding of the stretched chains and reduce $R_h$. On the other hand $R_g$ is rather costant for 0.15M NaCl and increasing for 0.01 M NaCl. This is possibly an effect of aggregation which cannot be easily decoupled from the measurements as in DLS where the relaxation time at the distribution maximum may be obtained by the CONTIN analysis. This is a sign that SLS measurements are very sensitive to the presence of aggregates in solution. This is also the reason why our Guinier diagrams do not appear perfectly linear. The importance of small angle scattering methods is proved here by its ability to distinguish between the different species even when they are organized in a hierarchical manner[21].

For the complexed micelles the amount of lysozyme can be calculated as follows[34]. Assuming that the scattered light from free lysozyme in solution is negligible then from $\frac{K_{pol}c_{pol}}{R(q=0,c)} = \frac{1}{M_w^{app}}$ the apparent molecular weight obtained has to be rescaled if we use polymer's parameters i.e. $K_{pol} = \frac{4\pi^2 n_0^2}{N_A \lambda^4}(\partial n/\partial c)_{pol}^2$ and $c_{pol}$. For $(\partial n/\partial c)_{pol}$ we use a weight average i.e. $(\partial n/\partial c)_{pol} = 0.5 \cdot (\partial n/\partial c)_{PnBA} + 0.5 \cdot (\partial n/\partial c)_{PAA}$ with[35] $(\partial n/\partial c)_{PnBA} = 0.134 ml/g$ and[36] $(\partial n/\partial c)_{PAA} = 0.14 ml/g$. For The additional mass percentage $w$ due to lysozyme on the micelle leads to a complexes molecular weight $M_w^{comp} = (1 + w) \cdot M_w^{mic}$, where $M_w^{mic}$ is the molecular mass of the

micelles before complexation. The concentration of the complexed particles is $(1+w)\cdot c_{pol}$ and their refractive index increment is $(\partial n/\partial c)_{comp} = \frac{1}{1+w}(\partial n/\partial c)_{pol} + \frac{w}{1+w}(\partial n/\partial c)_{lyso}$ with $(\partial n/\partial c)_{LYSO} = 0.153 ml/g$ [37]. From the equation $M_w^{app}\cdot K_{pol}\cdot c_{pol} = M_w^{comp}\cdot K_{comp}\cdot c_{comp}$ the mass percentage $w$ is obtained (equation 5).

$$w = \left(\sqrt{\frac{M_w^{app}}{M_w^{mic}}} - 1\right)\cdot \frac{(\partial n/\partial c)_{pol}}{(\partial n/\partial c)_{lys}} \qquad (5)$$

The resulting values for $Z_{lys}$ from SLS are also increasing with lysozyme concentration (tables 5 and 6). Nevertheless we would not expect higher lysozyme loading in LS experiments were $Z_{lys}$ is lower compared to SANS conditions. Additionally at lysozyme/PnBA-b-PAA mass ratio 4/10 and 0.15M NaCl (table 5) $Z_{lys}$ is much higher than in SANS and hence we conclude that micellar aggregation strongly affects apparent molecular weight. So although SLS follows the systematically increasing interaction between protein globules and micelles with high sensitivity it is difficult to extract $Z_{lys}$ quantitatively in the presence of two populations. Zeta potential measurements (tables 5 and 6) confirm the complexation of the negatively charged PnBA-b-PAA-2 micelles with positive charged lysozyme globules. The initially positive micelles reduce their absolute surface charge[38] as lysozyme is added. Surface charge reduction is another factor that contributes to the strong dependence of aggregation on lysozyme concentration. The zeta potential values are lower in absolute value in the solutions of high salt as expected because of the reduction of electrostatic interactions.

## 4. CONCLUSIONS

The self-assembly of three HOOC-PnBA-b-PAA-$C_{12}H_{25}$ amphiphilic polyelectrolytes is investigated in aqueous solutions. LS measurements reveal that PnBA-PAA-2 is the most well-defined micellar system. The SANS data analysis of PnBA-b-PAA-2 shows that it indeed forms core-shell micelles. For PnBA-b-PAA-1 the contribution of two separate species i.e. micelles and inter-micellar aggregates is observed. Complexation between PnBA-b-PAA-2 micelles with lysozyme occurs in mixed solutions as proved by LS measurements. SANS qualitatively describes both the loaded lysozyme amount per micelle and the formation of intemicellar aggregates as a function of lysozyme concentration. At 0.01M NaCl most of lysozyme is separated from solution, while at 0.15M there is a saturation of lysozyme loading at lower protein concentration. The morphology and shape of micelles do not change upon intermicellar aggregation which means that the aggregates formed are loose. Both the amount of loaded lysozyme and the hierarchical micelle organization can be tuned by the lysozyme and salt solution content. This study utilizes the power of scattering techniques to investigate the hierarchical organization of complex synthetic/biological hybrid self-assembled nanosystems as it qualitatively describes complexation of protein globules with single micelles and intermicellar aggregation.

## 5. SUPPORTING INFORMATION

Molecular characterization data of PnBA-b-PAA block copolymers (SEC and NMR).

## 6. ACKNOWLEDGEMENTS

The authors acknowledge financial support by the NANOMACRO 1129 project which is implemented in the framework of the Operational Program “Education and Life-long Learning” of the National Strategic Reference Program-NSRF (Action “ARISTEIA I”) and it is co-funded by the European Union (European Social Fund-ESF).

This research project has been supported by the European Commission under the 7th Framework Programme through the 'Research Infrastructures' action of the 'Capacities' Programme, NMI3-II Grant number 283883.

## 6. REFERENCES

1. Miyata, K.; Christie, R. J.; Kataoka, K., Polymeric micelles for nano-scale drug delivery. *React. Funct. Polym.* **2011,** 71, (3), 227-234.

2. Stuart, M. A. C.; Huck, W. T. S.; Genzer, J.; Muller, M.; Ober, C.; Stamm, M.; Sukhorukov, G. B.; Szleifer, I.; Tsukruk, V. V.; Urban, M.; Winnik, F.; Zauscher, S.; Luzinov, I.; Minko, S., Emerging applications of stimuli-responsive polymer materials. *Nat Mater* **2010,** 9, (2), 101-113.

3. Riess, G., Micellization of block copolymers. *Prog. Polym. Sci.* **2003,** 28, (7), 1107-1170.

4. Ballauff, M., Spherical polyelectrolyte brushes. *Prog. Polym. Sci.* **2007,** 32, 1135–1151.

5. Torchilin, V. P., Structure and design of polymeric surfactant-based drug delivery systems. *J. Controlled Release* **2001,** 73, (2–3), 137-172.

6. Kayitmazer, A. B.; Seeman, D.; Minsky, B. B.; Dubin, P. L.; Xu, Y., Protein-polyelectrolyte interactions. *Soft Matter* **2013,** 9, (9), 2553-2583.

7. Pedersen, J. S., Analysis of small-angle scattering data from colloids and polymer solutions: modeling and least-squares fitting. *Adv. Colloid Interface Sci.* **1997,** 70, 171-210.

8. Dmitri, I. S.; Michel, H. J. K., Small-angle scattering studies of biological macromolecules in solution. *Rep. Prog. Phys.* **2003,** 66, (10), 1735.

9. Cai, S.; Vijayan, K.; Cheng, D.; Lima, E. M.; Dische, D. E., Micelles of Different Morphologies—Advantages of Worm-like Filomicelles of PEO-PCL in Paclitaxel Delivery. *Pharm. Res.* **2007,** 24, (11), 2099-2109.

10. Lee, N. S.; Lin, L. Y.; Neumann, W. L.; Freskos, J. N.; Karwa, A.; Shieh, J. J.; Dorshow, R. B.; Wooley, K. L., Influence of Nanostructure Morphology on Host Capacity and Kinetics of Guest Release. *Small* **2011,** 7, (14), 1998-2003.

11. Sharma, G.; Valenta, D. T.; Altman, Y.; Harvey, S.; Xie, H.; Mitragotri, S.; Smith, J. W., Polymer particle shape independently influences binding and internalization by macrophages. *J. Controlled Release* **2010,** 147, (3), 408-412.

12. Rosenfeldt, S.; Wittemann, A.; Ballauff, M.; Breininger, E.; Bolze, J.; Dingenouts, N., Interaction of proteins with spherical polyelectrolyte brushes in solution as studied by small-angle x-ray scattering. *Phys. Rev. E* **2004,** 70.

13. Fitter, J.; Gutberlet, T.; Katsaras, J., *Neutron Scattering in Biology: Techniques and Applications*. Spinger: 2006.

14. Papagiannopoulos, A.; Karayianni, M.; Mountrichas, G.; Pispas, S.; Radulescu, A., Self-Assembled Nanoparticles from a Block Polyelectrolyte in Aqueous Media: Structural Characterization by SANS. *J. Phys. Chem. B* **2010,** 114, (22), 7482-7488.

15. Papagiannopoulos, A.; Zhao, J.; Zhang, G.; Pispas, S.; Radulescu, A., Thermoresponsive transition of a PEO-b-PNIPAM copolymer: From hierarchical aggregates to well defined ellipsoidal vesicles. *Polymer* **2013,** 54, (23), 6373-6380.

16. Chu, B., *Laser Light Scattering*. 2 ed.; Academic Press: New York, 1991.

17. Berne, B. J.; Pecora, R., *Dynamic Light Scattering, With Applications to Chemistry, Biology, and Physics*. Dover: Toronto, 2000.

18. Colombani, O.; Ruppel, M.; Burkhardt, M.; Drechsler, M.; Schumacher, M.; Gradzielski, M.; Schweins, R.; Müller, A. H. E., Structure of Micelles of Poly(n-butyl acrylate)-block-

poly(acrylic acid) Diblock Copolymers in Aqueous Solution. *Macromolecules* **2007,** 40, (12), 4351-4362.

19. Škvarla, J.; Zedník, J.; Šlouf, M.; Pispas, S.; Štěpánek, M., Poly(N-isopropyl acrylamide)-block-poly(n-butyl acrylate) thermoresponsive amphiphilic copolymers: Synthesis, characterization and self-assembly behavior in aqueous solutions. *Eur. Polym. J.* **2014,** 61, 124-132.

20. Buzin, A. I.; Pyda, M.; Costanzo, P.; Matyjaszewski, K.; Wunderlich, B., Calorimetric study of block-copolymers of poly(n-butyl acrylate) and gradient poly(n-butyl acrylate-co-methyl methacrylate). *Polymer* **2002,** 43, (20), 5563-5569.

21. Papagiannopoulos, A.; Karayianni, M.; Mountrichas, G.; Pispas, S.; Radulescu, A., Micellar and Fractal Aggregates formed by two Triblock Terpolymers with different arrangements of one Charged, one Neutral Hydrophilic and one Hydrophobic Block. *Polymer* **2015**, 63, 134-143.

22. Papagiannopoulos, A.; Zhao, J.; Zhang, G.; Pispas, S.; Radulescu, A., Thermoresponsive aggregation of PS–PNIPAM–PS triblock copolymer: A combined study of light scattering and small angle neutron scattering. *Eur. Polym. J.* **2014,** 56, 59-68.

23. Klein Wolterink, J.; van Male, J.; Cohen Stuart, M. A.; Koopal, L. K.; Zhulina, E. B.; Borisov, O. V., Annealed Star-Branched Polyelectrolytes in Solution. *Macromolecules* **2002,** 35, (24), 9176-9190.

24. Borisov, O. V.; Zhulina, E. B., Effects of ionic strength and charge annealing in star-branched polyelectrolytes. *Eur. Phys. J. B* **1998,** 4, 205-217.

25. Hammouda, B., Analysis of the Beaucage model. *J. Appl. Crystallogr.* **2010,** 43, (6), 1474-1478.

26. Sorensen, C. M., Light scattering by fractal aggregates: A review. *Aerosol Sci. Technol.* **2001,** 35, (2), 648-687.

27. Förster, S.; Hermsdorf, N.; Leube, W.; Schnablegger, H.; Regenbrecht, M.; Akari, S.; Lindner, P.; Böttcher, C., Fusion of Charged Block Copolymer Micelles into Toroid Networks. *J. Phys. Chem. B* **1999,** 103, (32), 6657-6668.

28. Lund, R.; Pipich, V.; Willner, L.; Radulescu, A.; Colmenero, J.; Richter, D., Structural and thermodynamic aspects of the cylinder-to-sphere transition in amphiphilic diblock copolymer micelles. *Soft Matter* **2011,** 7, (4), 1491-1500.

29. Egelhaaf, S. U.; Schurtenberger, P., Micelle-to-Vesicle Transition: A Time-Resolved Structural Study. *Phys. Rev. Lett.* **1999,** 82, 2804-2807.

30. Efimova, Y. M.; van Well, A. A.; Hanefeld, U.; Wierczinski, B.; Bouwman, W. G., On the neutron scattering length density of proteins in H2O/D2O. *Physica B Condens Matter* **2004,** 350, (1–3, Supplement), E877-E880.

31. Harding, S. E.; Rowe, A. J., Modelling biological macromolecules in solution: 1. The ellipsoid of revolution. *Int. J. Biol. Macromol.* **1982,** 4, (3), 160-164.

32. Wang, S.; Chen, K.; Kayitmazer, A. B.; Li, L.; Guo, X., Tunable adsorption of bovine serum albumin by annealed cationic spherical polyelectrolyte brushes. *Colloids Surf., B* **2013,** 107, 251-256.

33. Papagiannopoulos, A.; Meristoudi, A.; Hong, K.; Pispas, S., Kinetics of temperature response of PEO-b-PNIPAM-b-PAA triblock terpolymer aggregates and of their complexes with lysozyme. *Polymer* **2016,** 83, 111-115.

34. Azegami, S.; Tsuboi, A.; Izumi, T.; Hirata, M.; Dubin, P. L.; Wang, B.; Kokufuta, E., Formation of an Intrapolymer Complex from Human Serum Albumin and Poly(ethylene glycol). *Langmuir* **1999,** 15, (4), 940-947.

35. Katritzky, A. R.; Sild, S.; Karelson, M., Correlation and Prediction of the Refractive Indices of Polymers by QSPR. *J Chem Inf Comput Sci* **1998,** 38, (6), 1171-1176.

36. Golinska, M. D.; de Wolf, F.; Cohen Stuart, M. A.; Hernandez-Garcia, A.; de Vries, R., Pearl-necklace complexes of flexible polyanions with neutral-cationic diblock copolymers. *Soft Matter* **2013,** 9, (28), 6406-6411.

37. Carrara, S., *Nano-Bio-Sensing*. Springer: 2011.

38. Karayianni, M.; Pispas, S., Complexation of stimuli-responsive star-like amphiphilic block polyelectrolyte micelles with lysozyme. *Soft Matter* **2012,** 8, (33), 8758-8769.

**Table of Contents graphic**